

# Measuring full-field displacement spectral components using photographs taken with a DSLR camera via an analogue Fourier integral

Jaka Javh<sup>a</sup>, Janko Slavič<sup>a,\*</sup>, Miha Boltežar<sup>a</sup>

<sup>a</sup>*University of Ljubljana, Faculty of Mechanical Engineering, Aškerčeva 6, 1000 Ljubljana, Slovenia*

---

Cite as:

Jaka Javh, Janko Slavič, Miha Boltežar

Measuring full-field displacement spectral components using photographs taken with a DSLR camera via an analogue Fourier integral

Mechanical Systems and Signal Processing, Vol. 100, p. 17-27, 2018

DOI: 10.1016/j.ymsp.2017.07.024

## Abstract

Instantaneous full-field displacement fields can be measured using cameras. In fact, using high-speed cameras full-field spectral information up to a couple of kHz can be measured. The trouble is that high-speed cameras capable of measuring high-resolution fields-of-view at high frame rates prove to be very expensive (from tens to hundreds of thousands of euro per camera). This paper introduces a measurement set-up capable of measuring high-frequency vibrations using slow cameras such as DSLR, mirrorless and others. The high-frequency displacements are measured by harmonically blinking the lights at specified frequencies. This harmonic blinking of the lights modulates the intensity changes of the filmed scene and the camera-image acquisition makes the integration over time, thereby producing full-field Fourier coefficients of the filmed structure's displacements.

*Keywords:* DSLR camera, optical flow, modal analysis, photogrammetry, variable brightness, Lucas-Kanade

---

\*Corresponding author

*Email address:* janko.slavic@fs.uni-lj.si (Janko Slavič)

---

## 1. Introduction

Displacement measurements using high-speed cameras are increasingly being used in modal analysis, because they can produce a dense, simultaneous, full-field 3D measurement [1, 2].

Various image-processing techniques are being used to identify the displacements from image sequences. Some of the most commonly used techniques are: Gradient-Based Optical Flow [3–5], Digital Image Correlation [6], which is also gradient based, in fact the Lucas-Kanade method from [3] is the general form of DIC [7], Point Tracking [8] and Phase-Based methods [9].

Photogrammetry measurements using cameras enable many thousands or tens of thousands of points to be tracked simultaneously. The typical displacement resolution frame-to-frame is quoted at around 1/100 of a pixel and 1/10000 of a pixel in the amplitude spectrum [5], and is limited by the camera noise. By measuring with a stereoscopic camera set-up, three-dimensional displacements can be measured [10].

Probably the first use of photogrammetry for vibration measurements was a study carried out on the MIR space station [11]. More recent applications include civil engineering [12, 13], real-time measurements [14, 15] and large structures where the measurements have to be stitched together [16]. Cases of higher-frequency response measurements up to a couple of kHz have been reported in some recent papers as well [5, 17–23], where [17] covers the linear and non-linear responses compared to Continuous-Scan Laser Doppler Vibrometry, [18] is an example of model updating based on DIC data, [19] introduces interactive video manipulating based on the filmed structural responses, [20] identifies vibrations using phase-based motion magnification, [21] measures out-of-plane displacements based on fringe elongation, [22] uses DIC for thermo-structural coupling measurements and [23] gives a feasibility review of the DIC measurement for a case of hypersonic aircraft panels. Responses above a couple of kHz are problematic to measure, because they produce smaller displacements [24] and because of the high-speed camera's frame-rate limitations.

Mid-range high-speed cameras are typically capable of filming at a couple thousand frames per second (500–4000 fps) in the camera's full resolution, typically in the range of one or two mega-pixels ( $1024 \times 1024$  to  $1920 \times 1080$ ) and a 12-bit intensity resolution. Higher frame rates are possible when re-

ducing the image resolution. High-end cameras are capable of full resolution frame rates up to 20,000 fps. High-speed camera set-ups incorporating high-intensity lighting, lenses, etc. typically cost many tens of thousands of euros, and up to a few hundred thousand euros for a stereoscopic pair of higher-end cameras (3D measurements). To reduce the equipment costs, single-camera measurement approaches have been explored; the stereo information can be acquired with repeated measurements at different angles [25] or by using a dividing mirror, producing two viewing angles for a single camera [26, 27]. A simple approach to viewing fast phenomena is to use short pulses of light (strobe light) to produce still frames. Stroboscopes have been used since 1832 [28], where a slit in a disc would produce a flash of light and with it a discrete frame of an animated motion picture, in 1930 researchers used strobe lights to produce an analogue film high-speed camera capable of multiple thousand frames-per-second [29]. Some more recent examples of using stroboscopes to measure dynamics are: [30] where strobe lights were used to capture time instances of an oscillating wing and the displacements identified in 3D using multiple viewpoints and [31] where pulsated air jets were used to excite tissue and strobe lights made the response and with that tumors visible to the operator. A number of researchers have used lower-speed cameras to measure structural dynamics, by under-sampling and remapping the time instances [32], by using frequency zooming and allowing for aliasing [33], or by using multiple measurements with different sampling speeds to pinpoint actual aliased frequencies and showing that the spatial information is unaffected by aliasing [34], also the researchers that extracted sound from vibrations in videos [35] were able to use the rolling-shutter effect to sample high frequencies from a normal DSLR camera video. DSLR cameras have the benefit of producing images with a higher colour-intensity resolution (14-bit) and a higher pixel resolution (24 mega-pixels) at a cost of around 500–2000 euros.

This study introduces the Spectral Optical Flow Imaging (SOFI) measurement technique that uses low-speed image-acquisition cameras such as DSLR cameras to measure the individual displacement spectral components. By harmonically blinking the light source during the image acquisition, the displacement gets modulated on top of the blinking light, combined with the camera acquisition, which works by integrating the intensity over time, a single full-field displacement spectral component image is formed. The described technique, in fact, produces an analogue Fourier transform and each image for a different harmonic blinking of light produces separate Fourier

coefficients for the full camera field.

The text is organized as follows: Section 2 mathematically derives the proposed Spectral Optical Flow Imaging (SOFI) from the image-acquisition procedure and the Optical Flow theory, Section 3 demonstrates the use of the proposed method in structural dynamics, Section 4 discusses the limitations of the proposed method and the conclusions are drawn in Section 5.

## 2. Theoretical derivation

An image is formed as the illumination  $L$  is shown on a pattern with reflectance  $P(x, y)$  (or transmissivity in the case of transparency). The pattern  $P(x, y)$  is a function of the spatial coordinates  $x$  and  $y$  and reflects the light  $L$  to produce a radiance intensity  $r((x, y), L)$ :

$$r((x, y), L) = P(x, y) L \quad (1)$$

A camera produces an image of intensity values  $I(x, y)$  by integrating the radiance for individual pixels [36]. The pixels are discrete patches of photo-transistors that produce a linear response to the radiance illuminating them; henceforth, the spatial coordinates  $x$  and  $y$  are interpreted as pixel location indices. The image  $I((x, y), L)$  over pixels  $(x, y)$  at an illumination  $L$  equals the integral of the radiance  $r((x, y), L)$  over the camera's exposure time  $T_e$ :

$$I((x, y), L) = \int_0^{T_e} r((x, y), L) dt, \quad (2)$$

The camera's exposure time is the integration time that produces an image, and for DSLRs this typically ranges from 1/10000 s to 30 s.

Figure 1 shows a hypothetical radiance field plotted as a 3D function. A plane is plotted that dissects the radiance field in the direction of the radiance gradient, indicated with coordinate  $s$  for a point  $(x, y)$ . The thicker black line is the dissection of the radiance field with the plane and represents the radiance profile in the direction of the radiance gradient.

Figure 2 shows the intersection plane and the effect of a displacement and illumination change for a point  $(x, y)$ . It is clear that, assuming small displacements that are within the area of constant gradient, a displacement  $s$  will result in a radiance approximately equal to:

$$r((x, y) + s, L_0) = r((x, y), L_0) + s \nabla r((x, y), L_0), \quad (3)$$

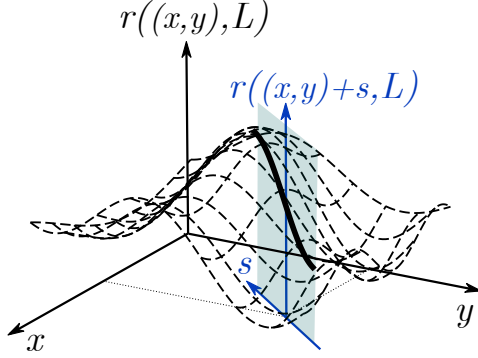


Figure 1: Plot of a radiance field over spatial dimensions  $(x, y)$

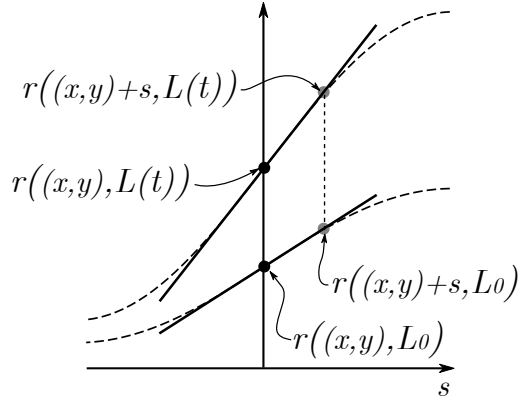


Figure 2: Gradient-oriented intersection plane from Figure 1 showing the effect of a varying illumination and the effect of displacements on the radiance

where  $\nabla r$  is the radiance gradient. Equation (3) is the basic Optical Flow equation, based on brightness conservation [3] (brightness is a generalised synonym of radiance) and is used to determine the motion from images (for more see [3, 5]), only in this paper the equation is written in terms of the radiance and not the image-intensity values for the purpose of further derivation where the brightness is assumed to vary.

For a varying illumination  $L(t)$ , the radiance will, according to Equation (1), increase proportionally:

$$r((x, y), L(t)) = L(t) P(x, y) = L(t) \frac{L_0}{L_0} P(x, y) = \frac{L(t)}{L_0} r((x, y), L_0) \quad (4)$$

By combining Equation (3) and Equation (4) the radiance of a point for a

time-varying displacement  $s((x, y), t)$  and illumination  $L(t)$  can be expressed as:

$$\begin{aligned} r\left((x, y) + s((x, y), t), L(t)\right) &= \frac{L(t)}{L_0} r\left((x, y) + s((x, y), t), L_0\right) = \\ &= \frac{L(t)}{L_0} \left( r((x, y), L_0) + s((x, y), t) \nabla r((x, y), L_0) \right) \end{aligned} \quad (5)$$

The integral of the left-hand side of Equation (5) over an exposure  $T_e$  (Equation (2)) produces the image taken for a varying illumination and displacement:

$$I((x, y) + s((x, y), t), L(t)) = \int_0^{T_e} r((x, y) + s((x, y), t), L(t)) dt \quad (6)$$

Assuming that the illumination  $L(t)$  changes harmonically in accordance with:

$$L(t) = L_0 + L_A \sin(\omega_l t) \quad (7)$$

and assuming that the displacements are the sum of various harmonics with angular frequencies  $\omega_n$ :

$$s((x, y), t) = \sum_n \left[ S_s((x, y), \omega_n) \sin(\omega_n t) + S_c((x, y), \omega_n) \cos(\omega_n t) \right], \quad (8)$$

the integral of the right-hand side of Equation (5) becomes:

$$\begin{aligned} &\int_0^{T_e} \frac{L(t)}{L_0} \left( r((x, y), L_0) + s((x, y), t) \nabla r((x, y), L_0) \right) dt = \\ &= \underbrace{\frac{L_0}{L_0} r((x, y), L_0) \int_0^{T_e} dt}_{\text{a)}} + \\ &+ \underbrace{\frac{L_A}{L_0} r((x, y), L_0) \int_0^{T_e} \sin(\omega_l t) dt}_{\text{b)}} + \\ &+ \underbrace{\frac{L_0}{L_0} \nabla r((x, y), L_0) \int_0^{T_e} s((x, y), t) dt}_{\text{c)}} + \\ &+ \underbrace{\frac{L_A}{L_0} \nabla r((x, y), L_0) \int_0^{T_e} \sin(\omega_l t) s((x, y), t) dt}_{\text{d)}} \end{aligned} \quad (9)$$

If  $\omega_n$  and  $\omega_l$  have periods whose multiple is  $T_e$ , then the integrals of the harmonics  $\sin(\omega_l t)$ ,  $\sin(\omega_n t)$  and  $\cos(\omega_n t)$  over  $T_e$  all equal zero. Therefore, the integrals b) and c) equal zero. The integral a) is the image when no motion is present and the illumination is constant at  $L_0$ :

$$I((x, y), L_0) = r((x, y), L_0) \int_0^{T_e} dt \quad (10)$$

The integral d) from equation (9) resembles the integral used to determine the Fourier series coefficients. The Fourier coefficients  $a_r$ ,  $b_r$  for  $r \in \mathbb{N}$  are determined as [37]:

$$a_r = \frac{2}{T} \int_{t_0}^{t_0+T} f(t) \cos\left(\frac{2\pi r t}{T}\right) dt \quad (11)$$

$$b_r = \frac{2}{T} \int_{t_0}^{t_0+T} f(t) \sin\left(\frac{2\pi r t}{T}\right) dt \quad (12)$$

Taking  $f(t)$  to be the function of the displacements over time  $s((x, y), t)$  Equation (12) can be rewritten as:

$$S_s((x, y), \omega_l) = \frac{2}{T_e} \int_0^{T_e} s((x, y), t) \sin(\omega_l t) dt \quad (13)$$

$T_e$  is chosen for the integral bounds, because  $T_e$  and  $\omega_l$  have been defined such that  $T_e$  is a multiple of the period of  $\omega_l$ .  $S_s((x, y), \omega_l)$  is the amplitude of the  $\sin(\omega_l t)$  harmonic of displacements  $s((x, y), t)$ .

Equation (9) paired with the left-hand side (6) and taking into account (10) and (13) reduces to:

$$I\left((x, y) + s((x, y), t), L(t)\right) = I((x, y), L_0) + \frac{L_A}{L_0} \nabla r((x, y), L_0) \frac{T_e S_s((x, y), \omega_l)}{2} \quad (14)$$

The product of the radiance gradient  $\nabla r$  and the exposure time  $T_e$  equals the reference image gradient, because the illumination  $L_0$  is constant and the radiance gradient  $\nabla r((x, y), L_0)$  does not incorporate any displacements  $s((x, y), t)$ :

$$\nabla I((x, y), L_0) = \int_0^{T_e} \nabla r((x, y), L_0) dt = T_e \nabla r((x, y), L_0) \quad (15)$$

and Equation (14) can be explained as:

$$\begin{aligned}
\underbrace{I((x, y) + s((x, y), t), L(t))}_{\text{blinking \& vibrations image}} &= \underbrace{I((x, y), L_0)}_{\text{reference image}} + \\
+ \underbrace{\frac{L_A}{L_0}}_{\text{illumination scaling}} \underbrace{\nabla I((x, y), L_0)}_{\text{reference image gradient}} \underbrace{\frac{S_s((x, y), \omega_l)}{2}}_{\text{displacement spectral component}} & \quad (16)
\end{aligned}$$

Therefore, by taking an image of a vibrating structure at a harmonically varying illumination (7), subtracting this image using a reference image of a stationary structure at a constant illumination  $L_0$  and scaling the result with the reference image gradient and the illumination scaling, a displacement spectral component  $S_s((x, y), \omega_l)$  can be obtained for every pixel:

$$S_s((x, y), \omega_l) = \frac{I((x, y) + s((x, y), t), L(t)) - I((x, y), L_0)}{\frac{1}{2} \frac{L_A}{L_0} \nabla I((x, y), L_0)} \quad (17)$$

By changing the frequency of the blinking lights other spectral components can be measured and by changing the phase of the lights from  $\sin(\omega_l t)$  to  $\cos(\omega_l t)$  the cosine amplitudes  $S_c((x, y), \omega_l)$  (Equation (11)) can be measured.

If the harmonic periods of  $\omega_l$  and  $\omega_n$  are not multiples of  $T_e$ , small errors will be imposed on the end results. The errors are analogue to the errors produced by windowing, which is sampling a signal in a finite window, thereby cutting off some information. Windowing and the spectral leakage associated with it are a common problem in signal processing [38].

It should be noted that the gradient at certain pixels can be insufficient to produce reliable results. A larger gradient will produce a greater sensitivity to displacements.

The displacement amplitudes  $S_s((x, y), \omega_n)$  and  $S_c((x, y), \omega_n)$  are displacements in the direction of the image gradient only; however, the displacements are typically two dimensional. As indicated by Equation (16) the image of a vibrating structure taken for a harmonically varying illumination equals the reference image (stationary structure and constant illumination) transformed by the scaled displacement amplitudes of the spectral component matching the illumination harmonic. Therefore, to identify the

2D displacements, the Lucas-Kanade Optical Flow [3] can be used on the "blinking & vibrations image" with respect to the reference image, which is possible because Lucas-Kanade is derived from linear-gradient assumptions and the 2D displacements are identified by using least-squares criteria on a subset of pixels (e.g., subsets of  $10 \times 10$  pixels). The 2D information is obtained because various pixels in the subset have various gradient directions.

According to Lucas-Kanade [3], the 2D displacements are determined by solving the system of equations:

$$\begin{Bmatrix} \Delta x \\ \Delta y \end{Bmatrix} = \begin{bmatrix} \sum (\frac{\partial I_0}{\partial x})^2 & \sum (\frac{\partial I_0}{\partial x} \frac{\partial I_0}{\partial y}) \\ \sum (\frac{\partial I_0}{\partial x} \frac{\partial I_0}{\partial y}) & \sum (\frac{\partial I_0}{\partial y})^2 \end{bmatrix}^{-1} \begin{Bmatrix} \sum ((I_1 - I_0) \frac{\partial I_0}{\partial x}) \\ \sum ((I_1 - I_0) \frac{\partial I_0}{\partial y}) \end{Bmatrix}, \quad (18)$$

where  $I_0$  is the reference image,  $I_1$  is the translated image,  $\partial I/\partial x$  indicates the gradient in the  $x$  direction (same goes for  $y$ ),  $\Delta x$  and  $\Delta y$  are the  $x$  and  $y$  displacement components and the summations indicate the convolutions over the subset, e.g., for a  $N \times N$  subset:

$$\sum \begin{pmatrix} \frac{\partial I_0}{\partial x} & \frac{\partial I_0}{\partial y} \end{pmatrix} = \sum_{k=-\frac{N}{2}}^{\frac{N}{2}} \sum_{l=-\frac{N}{2}}^{\frac{N}{2}} \begin{pmatrix} \frac{\partial I_0}{\partial x}(x+k, y+l) & \frac{\partial I_0}{\partial y}(x+k, y+l) \end{pmatrix} \quad (19)$$

In the case of SOFI, to obtain the 2D displacement components  $X_s((x, y), \omega_l)$  and  $Y_s((x, y), \omega_l)$ , image  $I((x, y) + s((x, y), t), L(t))$  should be used in place of  $I_1$  and the reference image  $I((x, y), L_0)$  should be used in place of  $I_0$ . Also, the result has to be scaled according to the illumination  $1/(L_A/L_0)$ .

### 3. Experimental validation

To test the proposed method two experiments were performed. The first experiment is intended to demonstrate the 2D SOFI by measuring the vibrations caused by the eccentricity of an electric motor. The DSLR SOFI measurement is compared to a high-speed camera measurement. The second experiment is the measurement of a cymbal excited with a pseudo-random (multisine) signal and is intended to show that selected spectral full-field displacement components can be measured using SOFI.

### 3.1. 2D Experiment

An electric motor was run at a PID-controlled frequency of rotation equal to 125 Hz. The PID control was established using an arduino micro-controller reading an optical tachometer signal. The integral component of the PID regulated the motor's phase, ensuring that the motor was synchronised with the blinking of the LED lights used to illuminate the filmed fixture. The PID kept the motor's rotation in phase with the lights with an error lower than  $4.5^\circ$  over the 3 s required to capture the reference image and two images with lights blinking in phase ( $\sin(2\pi f_l t)$ ) and a  $90^\circ$  phase ( $\cos(2\pi f_l t)$ ) required to produce the full-field spectral component at the frequency of the motor's rotation  $f_l = 125 \text{ Hz}$ . The DSLR exposure time was set to  $1/5 \text{ s}$  to be in line with the assumptions made in Section 2 and thereby avoid the windowing effects ( $1/5 \text{ s}$  is a multiple of  $1/f_l$ ). The other capture settings were fixed to produce an optimal exposure spanning the full 14-bit intensity resolution of the camera. The DSLR used was a Nikon D5300 set to capture 24 megapixel RAW images, which were later cropped to  $3576 \times 3616$  to fit the motor fixture. A high-contrast pattern sticker was placed on the motor fixture, to make the displacements more visible. The lights were proportionally controlled by an operational amplifier that compared the set blinking signal with the current passing through a single phototransistor placed in front of the LEDs. The proportional LED control accounted for the non-linearities in the LED power supply and the LED current to the illumination characteristic. The illumination scaling of the varying light was at  $I_A/I_0 = 1.25/1.5$ . The referenced blinking signal was generated using a NI9263 DAC card. The NI9263 DAC card also generated the trigger signal for the DSLR camera. The trigger signal was registered by an arduino, which triggered the DSLR via an IR-LED. The DSLR is a colour camera and captures the colour intensities in a Bayer pattern [39]. The images were transformed into black&white with spatial averaging of the pixel values. The averaging was done with a  $8 \times 8$  subset. This spatial averaging also serves to extend the area of constant gradient by filtering out the higher spatial frequencies in an image [3, 5].

The experimental set-up is shown in Figure 3. The high-speed camera in Figure 3 is present merely to monitor the process. The DSLR was later replaced with a Photron FASTCAM SA-Z high-speed camera and the measurement repeated at the same viewing angle as the DSLR (Figure 4).

Figure 5 shows the time series of the tachometer, the illumination measured by the phototransistor and the trigger signal for the DSLR. In the close-up section of Figure 5 the change in illumination phase from sine to

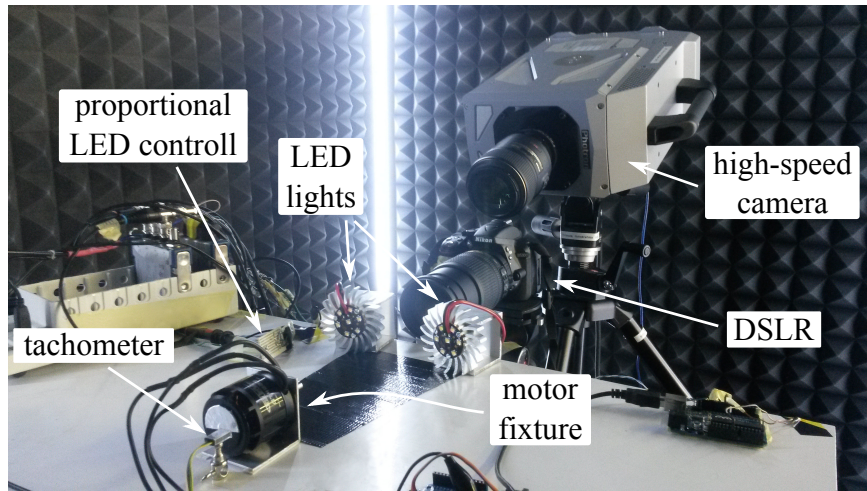


Figure 3: The SOFI electric motor experiment set-up

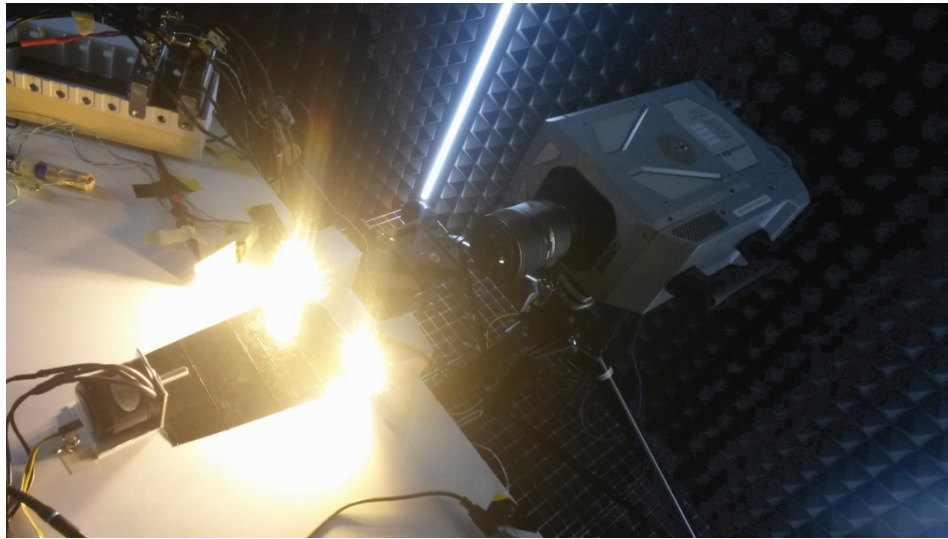


Figure 4: High-speed camera electric motor measurement

cosine is seen along with the trigger for the DSLR. The DSLR captured the image some arbitrary time after the trigger signal, which is why a sufficient time of 1 s was allocated for every image. The triggers for all three images (reference, sine phase and cosine phase) are shown in the full plot in Figure 5. The motor was running during the acquisition of the reference image, but the light was at a constant value. This is because such an image is approximately

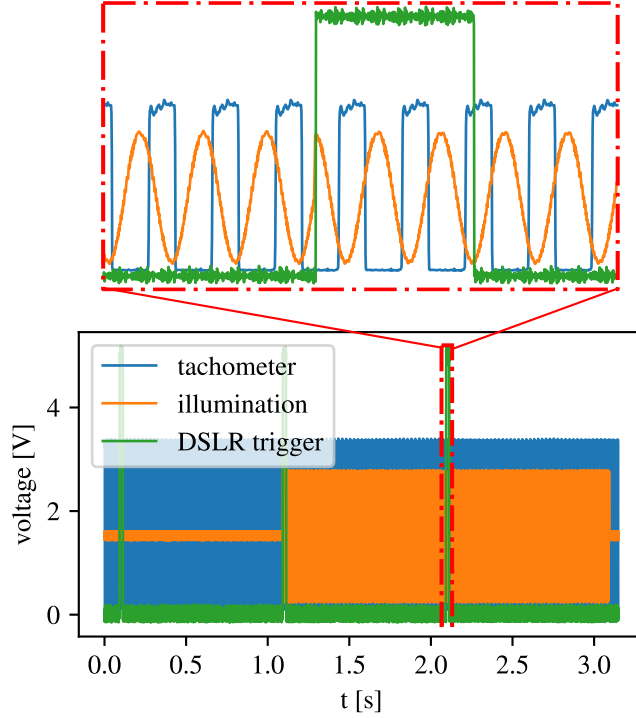


Figure 5: Monitored data of the electric motor experiment. Note that the DSLR trigger signal only indicates the trigger instance and not the entire exposure.

equal to the reference image:

$$\begin{aligned}
 I\left((x, y) + s((x, y), t), L_0\right) &= \\
 &= \int_0^{T_e} \left( r((x, y), L_0) + s((x, y), t) \nabla r((x, y), L_0) \right) dt \approx \\
 &\approx I((x, y), L_0), \tag{20}
 \end{aligned}$$

because the integral of the  $s((x, y), t) \nabla r((x, y), L_0)$  part is zero for harmonic motion when the exposure time  $T_e$  is a multiple of the periods of motion  $s(t)$  and the displacements are small (within the area of constant gradient). The data from Figure 5 was acquired by a NI9215 ADC card and was used for monitoring and for matching the phase with the measurements of the high-speed camera.

Figure 6 shows the displacement amplitudes measured using the DSLR and the high-speed camera. The yellow arrows represent the displacement

amplitudes for a 125 Hz sine phase and the red represents the cosine phase (colour figures available on-line). The SOFI and high-speed camera results

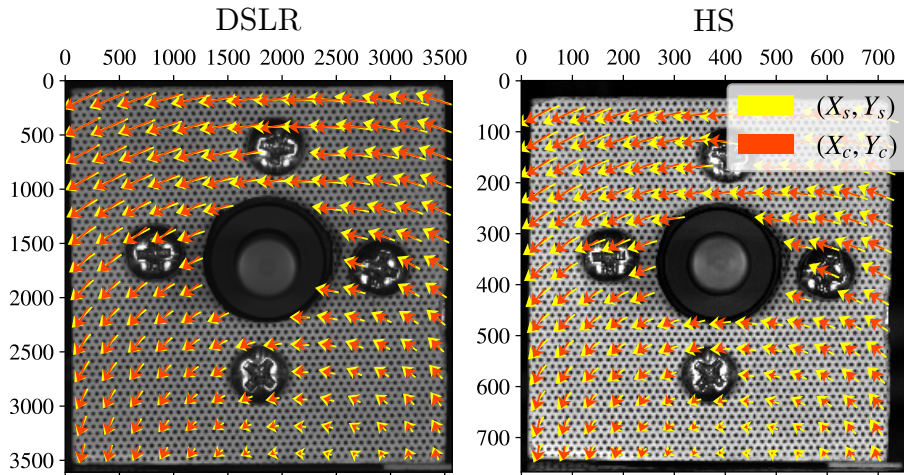


Figure 6: Displacement amplitudes of the motor fixture measured using a DSLR camera (SOFI), on the left, and using a high-speed camera (HS), on the right

were reconstructed into the trajectories caused by the frequency component. Figure 7 shows the reconstructed trajectories from the SOFI (DSLR) and the high-speed camera (HS) overlaid on the image captured by the DSLR. The ellipses are scaled by a factor of  $250\times$ . The agreement between the

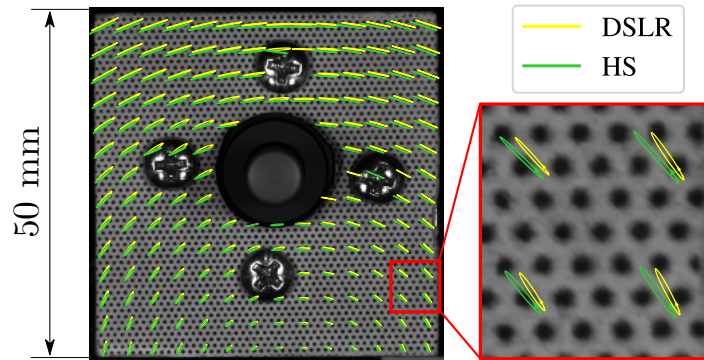


Figure 7: Overlaid reconstructed trajectories of the measured 125 Hz harmonic using the DSLR (SOFI) and the high-speed camera (HS). Trajectories are scaled by a factor of  $250\times$ .

measurements is good. Both measurements show a rotational motion with a

comparable scale. Small discrepancies between the HS and DSLR results are believed mostly to be the result of inconsistencies between the separate measurements, caused for instance by variations in the PID-regulated frequency of the motor rotation " $\omega_n$ ". The small discrepancies might also be caused by the windowing effects due to small deviations in the camera sampling with respect to the LED blinking frequency  $\omega_l$  and the camera's exposure time  $T_e$ , because the clocks were not physically synchronised. However, the frequency of rotation was set at a slightly smaller value ( $f = 124.1$  Hz) to match the 125 Hz frequency of the blinking of lights.

### 3.2. Multisine Experiment

A 14"/35 cm B8 Thin Crash cymbal was excited using a shaker (Figure 8). The excitation signal was a pseudo-random (multisine) signal with a band of



Figure 8: Cymbal SOFI experiment set-up

50 to 500 Hz and a period of 1 s. The force amplitude spectrum is shown in Figure 9 along with the response measured with a Laser Doppler Vibrometer (LDV) at a point close to the cymbal's edge. The velocity measured with the LDV was integrated to produce the displacement time series.

The SOFI measurement was automated to measure an array of frequencies chosen from the response peak locations ( $f = [56, 88, 112, 266, 349, 462, 466]$ ). The DSLR captured a reference, sine-blinking and cosine-blinking image for

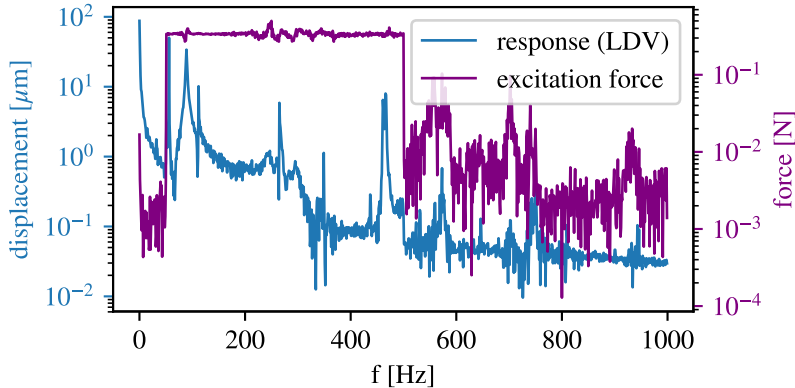


Figure 9: The excitation and response spectra for the cymbal experiment

each frequency. The image resolution was  $6000 \times 4000$  pixels. Figure 10 shows the monitored data (illumination, DSLR trigger, single point response (LDV) and excitation force) for two different blinking frequencies. The monitored data confirms that the response is repeatable, meaning that sequential measurements for different blinking frequencies and phases can be combined.

The images were analysed the same way as the electric-motor experiment and produced the full-field operational displacement fields seen in Figure 11. The displacements in Figure 11 are scaled in pixels, to scale them to out-of-plane deflections in micrometers an approximate conversion factor of  $76 \mu\text{m}/\text{pixel}$  can be used (based on the camera’s viewing angle and the pixel-to-length conversion using the cymbal’s size as a scale)

#### 4. Notes on the robustness of the proposed method

Obtaining good results proved to be hard, because the method is sensitive to outside influences and requires laboratory conditions to work. The requirements needed for the method to work are: small motion within the area of constant image gradient (typically smaller than one or a couple of pixels), a repeatable response to be able to combine sequential measurements, controlled harmonically varying light and harmonics fitting the exposure time  $T_e$  window.

The experiments were conducted in a dark room (anechoic chamber), because the illumination has to match the set profile. Both the motor and the cymbal had to be fixed to limit large rigid-body motion. Large displacements violate the small-displacements assumption, they might also cause windowing

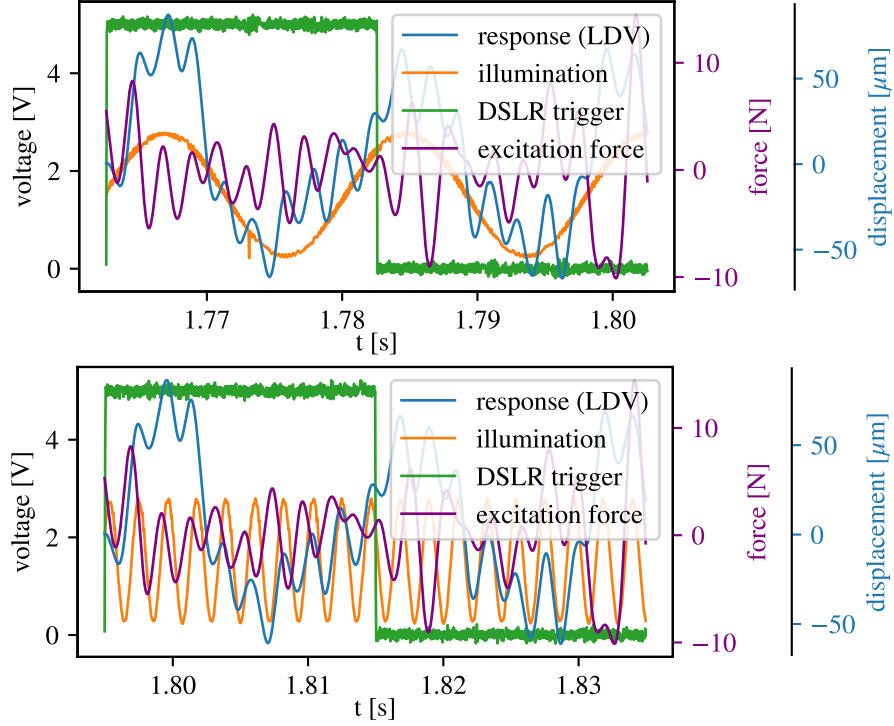


Figure 10: Monitored data for the cymbal experiment (upper - 56 Hz blinking, lower - 466 Hz blinking). Note that the DSLR trigger signal only indicates the trigger instance and not the entire exposure.

effects if their period is larger than the exposure time  $T_e$ . In the experiments, reference images were obtained during the motor's rotation and while the cymbal was vibrating (Equation (20)), because it proved that a shift can occur between a stationary reference image and the image during operation and this shift distorts the measured response. To measure both the sine and cosine phase amplitudes, two images need to be captured during the operation and the displacements must not change profile during this time. Attention has to be given to the acquisition settings and the synchronization of different systems.

## 5. Conclusion

The experiments prove that the Spectral Optical Flow Imaging (SOFI) method can be used to measure full-field displacement spectral components

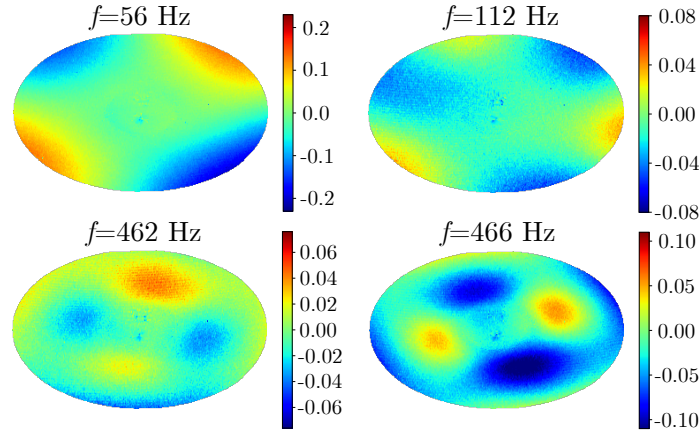


Figure 11: Full-field displacements amplitudes (sine phase) of a cymbal excited with a multi-sine signal (scale in pixels)

using affordable cameras such as DSLRs far above the frame rate of the camera.

The developed method is indifferent to the type of camera used as long as the camera’s settings can be controlled. In addition, better cameras (higher resolution, higher colour depth, lower noise) produce better results.

Spectral Optical Flow Imaging differs from stroboscopic measurements in that the stroboscopic light enables acquisition of instantaneous still frames, while the proposed method captures individual spectral components with every image taken. A strobe light will not accurately indicate a mode shape when a response is composed of multiple modes, while SOFI will.

The measurement of the running electric motor demonstrates a 2D measurement and validates the method via a comparison with a high-speed camera measurement and the cymbal experiment demonstrates the measurement of small, multi-sine, out-of-plane displacements up to 466 Hz, ranging in  $\mu\text{m}$ .

The method is sensitive to outside influences, such as light and vibrations; it is also sensitive to large and slow rigid-body motions or other shifts during the image acquisitions.

Compared to high-speed camera measurements the SOFI approach is much cheaper, although not as robust. DSLR cameras have a higher intensity resolution and a higher pixel resolution than high-speed cameras, but lack the capability to acquire a large number of images and the accompanying effect of a decrease in the spectral noise floor [5]. SOFI could be viable

in some operational modal analysis and in controlled experimental modal analysis.

## Acknowledgment

The authors acknowledge the partial financial support from the Slovenian Research Agency (research core funding No. P2-0263 and J2-6763).

## References

- [1] M. N. Helfrick, C. Niezrecki, P. Avitabile, T. Schmidt, 3D digital image correlation methods for full-field vibration measurement, *Mechanical Systems and Signal Processing* 25 (2011) 917–927.
- [2] J. Baqersad, P. Poozesh, C. Niezrecki, P. Avitabile, Photogrammetry and optical methods in structural dynamics - a review, *Mechanical Systems and Signal Processing* 86 (2017) 17–34.
- [3] B. Lucas, T. Kanade, An iterative image registration technique with an application to stereo vision, *International Joint Conference on Artificial Intelligence* (1981) 674–679.
- [4] B. Horn, B. Schunck, Determining optical flow, *Technical Symposium East. International Society for Optics and Photonics* (1981) 319–331.
- [5] J. Javh, J. Slavič, M. Boltežar, The subpixel resolution of optical-flow-based modal analysis, *Mechanical Systems and Signal Processing* 88 (2017) 89–99.
- [6] W. Peters, W. Ranson, Digital imaging techniques in experimental stress analysis, *Optical Engineering* 21 (3) (1982) 427–431.
- [7] M. A. Sutton, J. J. Orteu, H. W. Schreier, *Image Correlation for Shape, Motion and Deformation Measurements*, Springer Science & Business Media, 2009.
- [8] P. Olaszek, Investigation of the dynamic characteristic of bridge structures using a computer vision method, *Measurement* 25 (3) (1999) 227–236.

- [9] D. J. Fleet, A. D. Jepson, Computation of component image velocity from local phase information, *International journal of computer vision* 5 (1) (1990) 77–104.
- [10] P. F. Luo, Y. J. Chao, M. A. Sutton, W. H. Peters, Accurate measurement of three-dimensional deformations in deformable and rigid bodies using computer vision, *Experimental Mechanics* 33 (2) (1993) 123–132.
- [11] M. Gilbert, S. Welch, STS-74/MIR photogrammetric appendage structural dynamics experiment, *Proceedings of the 1996 37th AIAA/ASME/ASCE/AHS/ASC Structures Structural Dynamics and Materials Conference* (1996) 1594–1604.
- [12] E. Caetano, S. Silva, J. Bateira, Vision system for vibration monitoring of civil engineering structures, *Experimental Techniques* 35 (4) (2011) 74–82.
- [13] B. K. Oh, J. W. Hwang, Y. Kim, T. Cho, H. S. Park, Vision-based system identification technique for building structures using a motion capture system, *Journal of Sound and Vibration* 356 (2015) 72–85.
- [14] J. Guo, C. Zhu, Dynamic displacement measurement of large-scale structures based on the lucaskanade template tracking algorithm, *Mechanical Systems and Signal Processing* 66 (2016) 425–436.
- [15] B. Pan, L. Tian, X. Song, Real-time, non-contact and targtless measurement of vertical deflection of bridges using off-axis digital image correlation, *NDT&E International* 79 (2016) 73–80.
- [16] P. Poozesh, J. Baqersad, C. Niezrecki, P. Avitabile, E. Harvey, R. Yarala, Large-area photogrammetry based testing of wind turbine blades, *Mechanical Systems and Signal Processing* 86 (2017) 98–115.
- [17] D. A. Ehrhardt, M. S. Allen, S. Yang, T. J. Beberniss, Full-field linear and nonlinear measurements using continuous-scan laser doppler vibrometry and high speed three-dimensional digital image correlation, *Mechanical Systems and Signal Processing* 86 (2017) 82–97.
- [18] W. Wang, J. E. Mottershead, A. Ihle, T. Siebert, H. R. Schubach, Finite element model updating from full-field vibration measurement using

- digital image correlation, *Journal of Sound and Vibration* 330 (8) (2011) 1599–1620.
- [19] A. Davis, J. G. Chen, F. Durand, Image-space modal bases for plausible manipulation of objects in video, *ACM Transactions on Graphics (TOG) - Proceedings of ACM* 34 (6) (2015) .
- [20] J. G. Chen, N. Wadhwa, Y. J. Cha, F. Duran, T. Freeman, O. Buyukozturk, Modal identification of simple structures with high-speed video using motion magnification, *Journal of Sound and Vibration* 345 (2015) 58–71.
- [21] S. Zhong, J. Zhong, Q. Zhang, N. Maia, Quasi-optical coherence vibration tomography technique for damage detection in beam-like structures based on auxiliary mass induced frequency shift, *Mechanical Systems and Signal Processing* 93 (2017) 241–254.
- [22] R. Perez, G. Bartram, T. Beberniss, R. Wiebe, S. M. Spottswood, Calibration of aero-structural reduced order models using full-field experimental measurements, *Mechanical Systems and Signal Processing* 86 (2017) 49–65.
- [23] T. J. Beberniss, D. A. Ehrhardt, High-speed 3D digital image correlation vibration measurement: Recent advancements and noted limitations, *Mechanical Systems and Signal Processing* 86 (2017) 35–48.
- [24] J. Javh, J. Slavič, M. Boltežar, High frequency modal identification on noisy high-speed camera data, *Mechanical Systems and Signal Processing* 98 (2018) 344–351.
- [25] T. G. Ryall, C. S. Fraser, Determination of structural modes of vibration using digital photogrammetry, *Journal of Aircraft* 39 (1) (2002) 114–119.
- [26] M. Pankow, B. Justusson, A. M. Waas, Three-dimensional digital image correlation technique using single high-speed camera for measuring large out-of-plane displacements at high framing rates, *Applied Optics* 49 (17) (2010) 3418–3427.
- [27] L. Yu, B. Pan, Single-camera high-speed stereo-digital image, *Mechanical Systems and Signal Processing* 94 (2017) 374–383.

- [28] S. Stampfer, *Die stroboscopischen Scheiben; oder, Optischen Zauberscheiben: Deren Theorie und wissenschaftliche Anwendung*, Trentsensky & Vieweg, 1833.
- [29] H. E. Edgerton, Stroboscopic moving pictures, *Electrical Engineering* 50 (5) (1931) 327–329.
- [30] T. G. Ryall, C. S. Fraser, Determination of structural modes of vibration using digital photogrammetry, *Journal of aircraft* 39 (1) (2002) 114–119.
- [31] M. Kaneko, C. Toya, M. Okajima, Active strobe imager for visualizing dynamic behavior of tumors (2007) 3009–3014.
- [32] Y. Liu, H. Gao, J. Zhuge, J. Zhao, Research of under-sampling technique for digital image correlation in vibration measurement, *Shock & Vibration, Aircraft/Aerospace, Energy Harvesting, Acoustics & Optics* 9 (2017) 49–58.
- [33] J. Javh, M. Brumat, J. Slavič, M. Boltežar, A high-speed camera measurement set-up for deflection shape analysis, *Proceeding of ISMA2016-USD2016*, (2016) 1043–1050.
- [34] Y. Yang, C. Dorn, T. Mancini, Z. Talken, S. Nagarajaiah, G. Kenyon, C. Farrar, D. Mascarenas, Blind identification of full-field vibration modes of output-only structures from uniformly-sampled, possibly temporally-aliased (sub-Nyquist), video measurements, *Journal of Sound and Vibration* 390 (2017) 232–256.
- [35] A. Davis, M. Rubinstein, N. Wadhwa, G. Mysore, F. Durand, W. T. Freeman, The visual microphone: Passive recovery of sound from video, *ACM Transactions on Graphics (Proc. SIGGRAPH)* 33 (4) (2014) 1–10.
- [36] M. Burke, *Image Acquisition Handbook of machine vision engineering: Volume 1*, Chapman & Hall, Boundary Row, London, 1996.
- [37] K. F. Riley, M. P. Hobson, S. J. Bence, *Mathematical Methods for Physics and Engineering*, Cambridge University Press, 2006.
- [38] K. Shin, J. Hammond, *Fundamentals of signal processing for sound and vibration engineers*, John Wiley & Sons, 2008.
- [39] M. Brown, *Advanced Digital Photography*, Media Publishing Pty, 2004.